



Optical Retardation based on Tunneling-Induced Transparency in Quantum Dot Slow light Devices

Hossein Mardani¹ · Hassan Kaatuzian¹ · Bahram Choupanzadeh¹

Received: 25 October 2021 / Accepted: 18 June 2022 / Published online: 20 July 2022
© The Author(s), under exclusive licence to Springer Science+Business Media, LLC, part of Springer Nature 2022

Abstract

In this article, we investigate the effect of reducing the speed of light by applying an electric field. This method is called tunneling-induced transparency (TIT). The research is based on the quantum structure of the ten layers of gallium arsenide and quantum dots of indium arsenide. We simulate and examine the transmission capacity of this device in terms of passing the wavelengths of the optical window. By widening the frequency transparency window, we can increase the light transmission limit of the probe. After passing the electric field of the probe light through a device based on quantum dots, the group velocity is predicted to be decreased by about 3 million times, which is about twice as much as similar work reported before Borges et al. (Phys Rev B 85:115425, 2012). Our main device is made from gallium arsenide, the dots are made from indium arsenide, and their surface distance from each other is 50 nm.

Keywords Tunneling-induced transparency · Slow light · Detuning frequency · Double quantum dot

1 Introduction

The speed of light in a vacuum is about 300,000 km/sec. Despite this high value, for optical retarding applications, we still need to develop slow light devices to reduce light velocity even to the speed of a car. The set of the phenomenon to reduce the speed of light to this

This article is part of the Topical Collection on Numerical Simulation of Optoelectronic Devices.

Guest edited by Slawek Sujecki, Asghar Asgari, Donati Silvano, Karin Hinzer, Weida Hu, Piotr Martyniuk, Alex Walker and Pengyan Wen.

✉ Hassan Kaatuzian
hsnkato@aut.ac.ir

Hossein Mardani
mard@aut.ac.ir

Bahram Choupanzadeh
choupanzadeh@aut.ac.ir

¹ Photonics Research Lab (PRL), Electrical Engineering Department, Amirkabir University of Technology, Tehran, Iran

extent is called slow light. Standard methods for achieving slow light include Stimulated Brillouin Scattering (SBS), Electromagnetically-Induced Tunnelling (EIT), and Tunneling-Induced Transparency (TIT). Slow light may be used for beam splitter construction (Xiao et al. 2008), quantum computation, optical storage, and quantum telecommunications (Harris 1997; Marangos 1998). Quantum dots are usually structures with a radius between 2 up to 10 nm.

This structure limits energy transfer layers because it comprises a limited number of atoms, thus limiting the transmission wavelengths. Quantum dots have many applications in new generation screens and cancer detection.

The method we consider here to slow the speed of light is the TIT method, with the ability to reduce the speed of light up to retardation by several million. The probe light is applied in a quantum dot structure, and if the conditions of induction transparency are created, light can pass through the device with small losses. Since the speed of light in the quantum dot structure can be slower than other quantum structures, we use this structure in our project. The Λ system is also used in the EIT method. The EIT is a phenomenon for creating slow light and allows the laser light to pass through the dense material by the control laser. In the Λ type system, the EIT requires two ground states, which are not directly paired, and must be state-mediated by coupling the states (Kaatuzian 2020a). Whenever we use electron tunneling between quantum structures instead of a control laser, the tunneling-induced transparency method produces slow light.

In this work, as shown in Fig. 1, an electric field must be applied along the growth axis of the quantum growth layers; thus, by changing the energy levels of the carriers in the conduction bands and capacity, tunneling resonance can be reached.

The material of the potential barrier structure in this device is indium arsenide, and the main structure of the layers is gallium arsenide.

The first part introduces the device under test and its environmental and physical conditions.

The second part deals with the theory and equations governing the devices. Further, in the third part of the article, simulating physically available parameters, we improve the slow down and Q-factor parameters in the discussion of optical telecommunications.

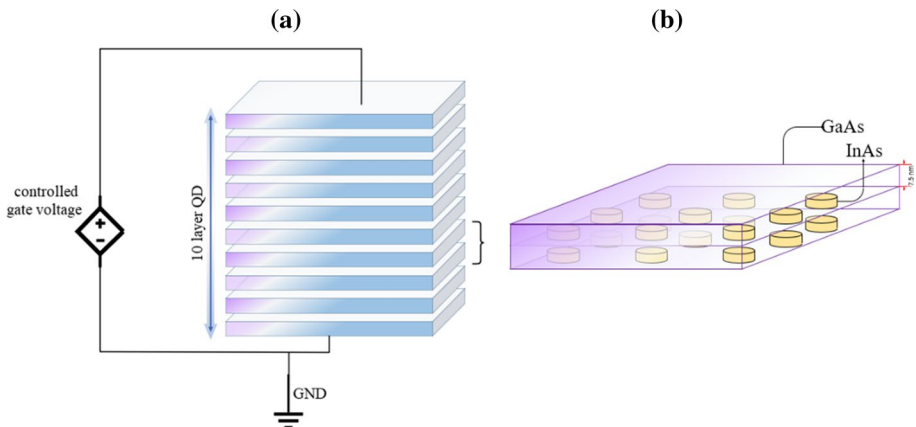


Fig. 1 (a) The direction of the electric force caused by the applied electric field leading to the energy level of the electric carrier tilt in the quantum structure; (b) The cross-section of the QD structure

1.1 Quantum dot structure selection

In terms of dimensional constraints, quantum boxes are divided into three categories: quantum boxes with limited movement of carriers in one dimension, quantum wires with limited movement in two dimensions, and quantum dots with limited movement in three dimensions. In this paper, we use the Quantum Dots (QDs) Structure.

The advent of quantum hardware has revolutionized computers; thus, a new generation of computers called all-optical computing systems has entered the field. In digital computers, due to semiconductor flow problems, there are limitations at reducing the dimensions, while in all-optical systems, there are no such limitations, and the computing speed increases Finds.

The coupling of photons can also be used in slow light, creating the capacity to generate pairs of interconnected photons to be used in quantum computers with an advantage over conventional computers. At present, we are at the beginning of the development path of such computers (Kaatusian 2020b).

2 Theory

2.1 Selected quantum structure

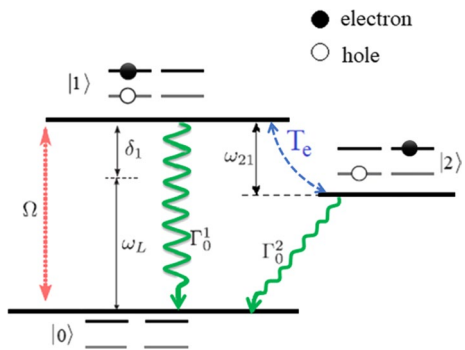
Our quantum dot structures are cylinders with a radius of 9 nm and a height of 3.5 nm. The distance of quantum dots from each other in a layer is about 50 nm, and it has a height of 7.5 nm in line with its growth axis. Figure 2 shows three states of the TIT method and related parameters plotted. Ω indicates the frequency of the Rabi transition from state $|1\rangle$ to $|0\rangle$, and T_e is the tunneling coupling. Γ_j^i is the decreasing rate of the electron carriers from the high energy level $|i\rangle$ to the low energy level $|j\rangle$, and ω_{ij} represents the frequency of the energy level difference between the states i and j . Effective dephasing parameters (Γ_1, Γ_2) can be available by holding Γ_0^1, Γ_0^2 through the following equations (Borges et al. 2012).

$$\Gamma_1 = 0.5(\Gamma_0^1 + \gamma_1), \Gamma_2 = 0.5(\Gamma_0^2 + \gamma_2) \tag{1}$$

where γ_1 and γ_2 are pure dephasing rate or virtual transition (Kaatusian 2020b); here Γ_2 is assumed to be much smaller than Γ_1 ($\Gamma_2 = \Gamma_1/1000$).

These coefficients also depend on the geometry of the dots, which in the present work are cylindrical disks. Other factors can affect dephasing, one of which is thermal excitation,

Fig. 2 Diagram of triple Λ state in which electrons could tunnel from the barrier; Γ coefficients indicated by the green helix showing the direct and indirect diffusion parameters



indicating that the device’s temperature should be kept as low as possible (50 to 80 K); for solving this problem, we can use liquid nitrogen (Hayashida et al. 2003).

V represents the volume of a quantum dot; here, it is the volume of a quantum cylinder equal to $8.9 \times 10^{26} \text{m}^3$. μ or the electric dipole moment is defined between states $|0\rangle$ to $|1\rangle$ in $e \text{ \AA}$ units (Chang-Hasnain et al. 2003).

In order to check the graphic characteristics around the central frequency, we use the definitions of detuning frequency, and based on which, δ_1 is defined as $\delta_1 = \omega_{01} - \omega_L$ and δ_2 as $\delta_2 = \delta_1 + 2\omega_{21}$.

2.2 Hamiltonian equation extraction

Any operator with two definite properties of the matrix being positive with one as the sum of its original diameter is mathematically called the density matrix. Since the density matrix system (ρ) has 3 states, it has 3 rows and 3 columns, and ρ_{10} is the component of our attention.

$$\rho_{10} = \frac{(\delta_1 + \delta_2) + 2j\Gamma_2}{(j\delta_1 - \Gamma_1)(j(\delta_1 + \delta_2) - 2\Gamma_2) + 2T_e^2} \tag{2}$$

The mixed acceptance parameter is proportional to the density, and according to Eq. 3, the smaller quantum dot volume shrinks V (the volume of a quantum dot) and increases the acceptability size.

$$\chi = \frac{\Gamma_{opt}}{V} \frac{|\mu_{10}|^2}{\epsilon_0 \hbar \Omega} \rho_{10} \tag{3}$$

Γ_{opt} or optical confinement is a parameter that depends on the waveguide property, indicating the ratio of the laser light mode inside the active substance in our dot structures.

2.2.1 Two-State System

The tunneling coefficient is itself a function of several parameters that depend on d (the distance between dots), E (electric field), V(voltage), and m_{eff}^* (the effective mass of electric carriers).

$$T_e = \text{function of} \left(d, E, V, m_{eff}^* \right) \tag{4}$$

$$T_e = 2aV_0BCe^{-2\beta d} = 3.5 \times 10^{-9} V_0BCe^{-1.5 \times 10^{-8} \beta} \tag{5}$$

If T_e or tunneling strength is zero, there is no control signal; therefore, there is a two-state system that carriers can be transferred from 0 to 1 only with a laser probe. This causes a single peak in the absorption diagram, and the input light is subject to many losses. The phase increased coefficients and the group indexes are obtained according to the detuning frequency. For electrons, the effective mass of gallium arsenide is assumed to be equal to 0.06 mass of electrons (Abdolhosseini et al. 2017).

When a laser probe is applied to a material containing quantum dots, it separates and energizes the electron inside the quantum dot, creating an internal exciton. Excitons are divided into two categories of Fresnel Vanier and Frankel in terms of structure and energy

level. The energy of the excitons is due to the Coulomb attraction between two dissimilar electrons and holes (Ficek and Swain 2002). Then, applying a suitable electric field to this system causes the electron to be located in the conduction layer of the dots to tunnel to the adjacent dot and create an indirect exciton. Figure 3 shows an intensified state of electron motion between two potential dots. According to the Hamiltonian equation, the electron energy is obtained from the opposite relation.

$$H = \sum_{i=0}^2 \hbar\omega_i|i\rangle\langle i| + T_e(|1\rangle\langle 2| + |2\rangle\langle 1|) + \frac{\mu_{01}E}{2} (e^{-j\omega_L t}|0\rangle\langle 1| + e^{j\omega_L t}|1\rangle\langle 0|) \quad (6)$$

It shows the rate of absorption and refraction, as well as the speed of the group, in the case that the device is not under any external field. In this case, the laser probe experiences a lot of losses, and there is not a good output. The group index also has a negative value around the resonance frequency.

Without an external electric field signal, the output light has a weak gain, and the slow down factor is less than 10 thousand; however, by applying the appropriate electric field and getting output from the MATLAB simulator, the laser losses of the probe reduce and the group index increases to a high level, the numerical (values of which we will review in the next section).

Figure 4 shows the absorption curves, phase enhancement coefficient, and optical deceleration coefficient in terms of detuning frequency, in simulation by sweeping other variables such as tunneling and ω_{21} coefficients, the best point selected to achieve maximums SDF coefficient. We simulate the selection and the three functions around the detuning coefficient by Eq. 2.

2.3 Three-state system

In the index group diagram, we see different positive and negative values. Positive values are seen with a finite distance on either side of the central frequency.

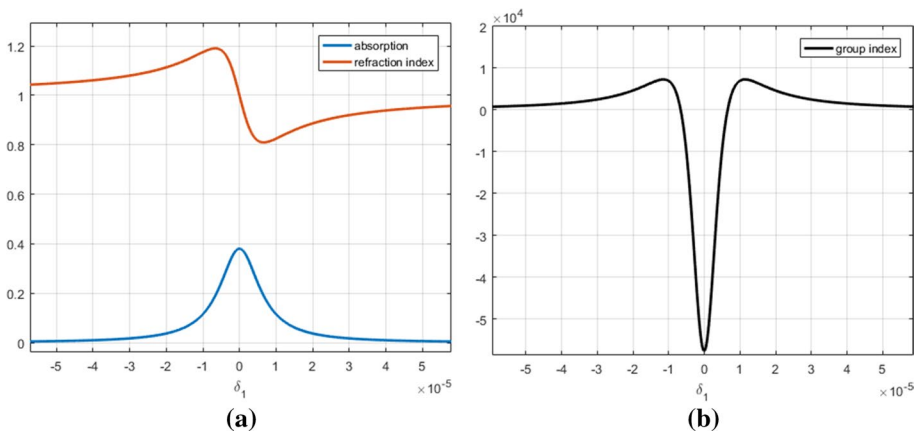


Fig. 3 (a) Absorption and refraction index curves without the external electric field; (b) Corresponding group index curve

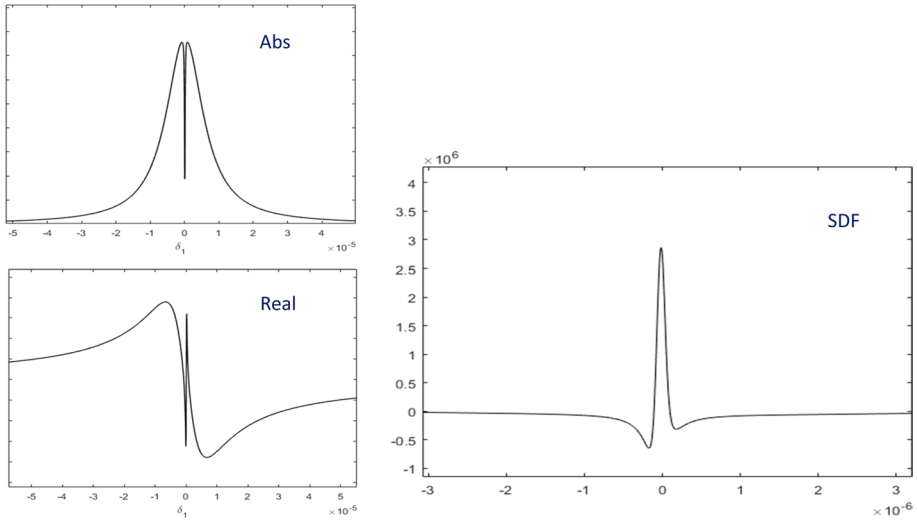


Fig. 4 Specifications of group index after applying the electric field; General absorption curves, phase index, and deceleration coefficient in the range around the induction transparency window of tunneling

As seen in Fig. 5, by adopting characteristics around the axis $\omega 21 + \delta 1 = 0$, one can expect the most changes in the real and imaginary parts of n (refraction index) concerning the detuning frequency, thus looking for the maximum SDF at these points.

According to Fig. 5, the amount of transparency window is wider as the tunneling coefficient increases; this is also proved with the help of simulation. Now, by these parameters, we can show the absorption profiles and the real part of the susceptibility in the TIT conditions and the tunneling strength T_e equal to half Γ_1 on the diagrams in Fig. 6.

$$\frac{c}{V_g} = n + \omega_L \frac{dn}{d\omega_L} = n - \omega \left. \frac{dn}{d\delta_1} \right|_{\omega=\omega_{01}} \tag{7}$$

$$n(\omega_L) = \sqrt{\frac{\epsilon' + \sqrt{\epsilon'^2 + \epsilon''^2}}{2}} \tag{8}$$

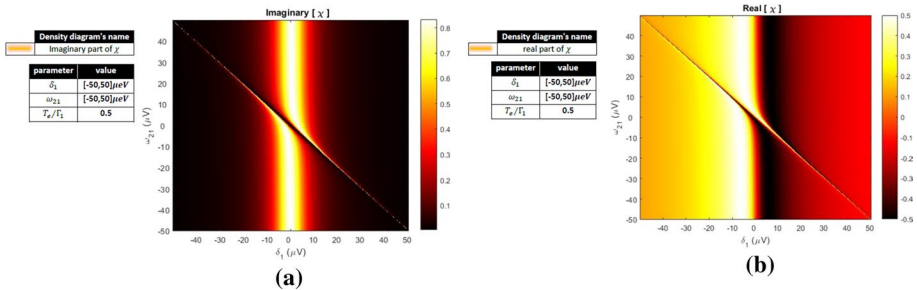


Fig. 5 (a) The imaginary part of the susceptibility; (b) the real part of the susceptibility Numerical values are marked in color as a density diagram. Larger values are seen with brighter colors

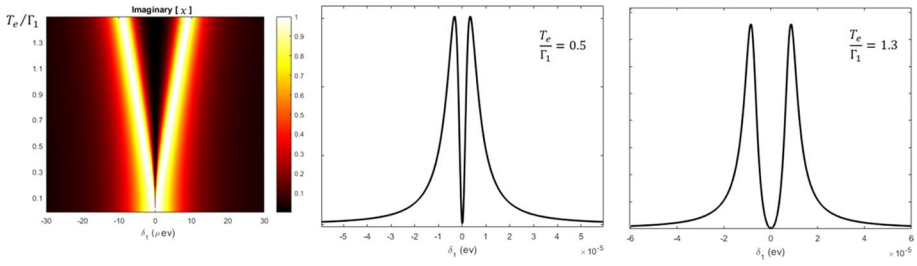


Fig. 6 Imaginary parts of χ as a function of detuning

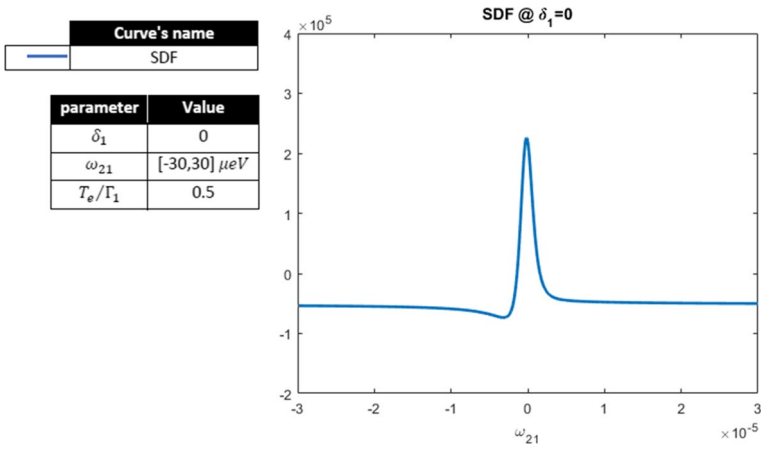


Fig. 7 SDF at $\delta_1 = 0$ and $T_e = \Gamma_1/2$

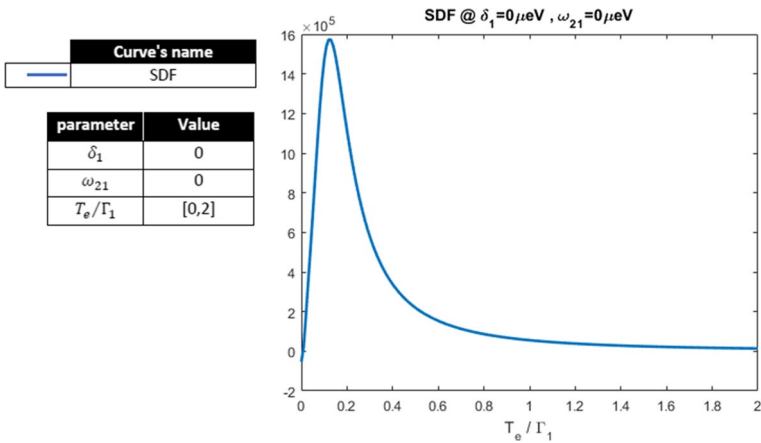


Fig. 8 SDF at $\omega_{21} = 0$ and $\delta_1 = 0$

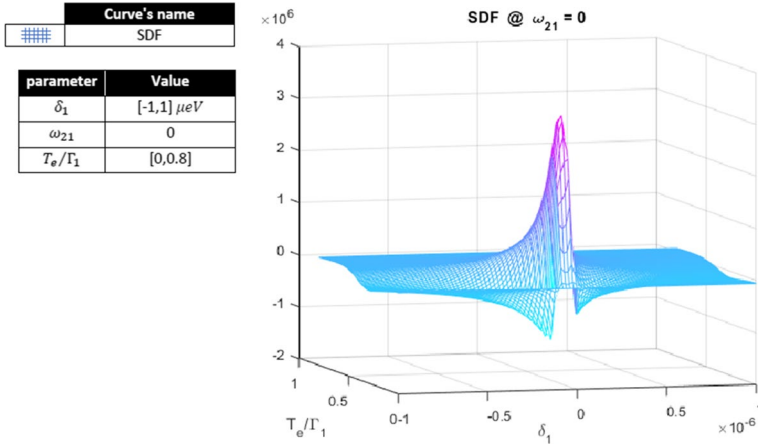
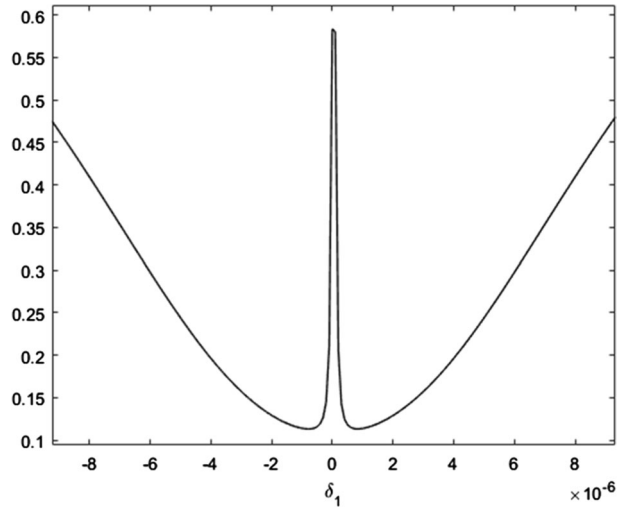


Fig. 9 SDF at $\omega_{21} = 0$

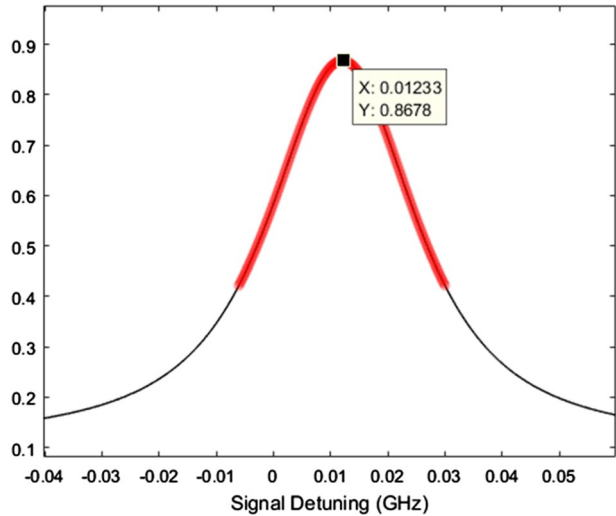
Fig. 10 Transmission intensity of light-based arbitrary intensity scale;



$$\epsilon' = 1 + 4\pi Re[\chi], \epsilon'' = 4\pi Im[\chi] \tag{9}$$

The central frequency for such a device is 1.6 electron volts, which is equivalent to the energy of an electromagnetic wave with a wavelength of 775 nm. Such a wavelength range is commonly used for CD-ROM, which uses infrared frequency (Fleischhauer et al. 2005).

Fig. 11 The window of light at the central frequency. The telecommunication bandwidth calculated in the diagram by the FWHM method is obtained and displayed in red during this interval



3 Slow light parameters

3.1 Improvement of SDF

SDF coefficient (Slow Down Factor of group velocity) shows the difference between group speed in the device and a vacuum; SDF is obtained through the following equation (Fritze et al. n.d):

$$SDF = \frac{n(\omega) + \omega \frac{\partial n}{\partial \omega}}{1 - \frac{\omega}{c} \frac{\partial n}{\partial k}} \tag{10}$$

where K represents the propagation constant on the waveguide. The SDF parameter must be checked and simulated around the central frequency ω_0 . For this purpose, by changing the detuning frequency (ω_{21}) and using Eq. 10, we draw the SDF value in terms of ω_{21} with the conditions $T_e/\Gamma_1 = 0.5$ and $\delta_1 = 0$.

Then, we do the same with the assumption that $\delta_1 = 0$ is constant and the coefficient $\frac{T_e}{\Gamma_1}$ is variable and again repeat the simulations and draw it respectively at Fig. 7 and Fig. 8.

In order to get a better conclusion and a greater SDF than the two variable parameters, the SDF diagram is drawn in terms of two parameters δ_1 and $\frac{T_e}{\Gamma_1}$, with identifying its peak point in the output plot as in Fig. 9.

The functions of slow light devices may be multiplexed data entering the device from multiple transmission lines, buffering light signals, preventing pulse interference, and controlling or switching the optical path.

Therefore, to use the application of hardware buffering, we must calculate the delay values in terms of various physical parameters; we have the solution for the delay as (Li et al. 2014):

$$T_s = \frac{L_D S \sqrt{\epsilon_{back}}}{c} \tag{11}$$

Where L_D is the length of the active path through which light passes. In the present paper, $L_D = 75\text{nm}$, S is equal to the deceleration coefficient, and c is the speed of light in a vacuum. The parameter ϵ_{back} is also equivalent to the electrical conductivity of the background of the material, and $\epsilon_{back} = 13.1$.

To compare different amounts of storage time, its calculation based on physical parameters is classified in Table 1.

3.2 Bandwidth frequency

To calculate the bandwidth frequency, we need a quantity that measures the intensity of the light emitted in terms of different frequencies. Therefore, we must obtain the transmissivity pattern from the absorption diagram. If we show the transmissivity coefficient with T and the absorption with A , we have the following relation:

$$T = \frac{I_m}{I_o} = 10^{-A} \quad (12)$$

As a result, the transmissivity diagram is drawn as Fig. 10.

As observed in the diagram, the input light with a maximum amplitude of 0.6 can be transmitted to the output, and the rest is spent on losses inside the device.

In optical applications, there are two types of bandwidth: power and optical bandwidths. In the former, the power cut-off frequency is calculated, while in the latter, the light intensity of the parameter is considered.

Due to the quadratic power with light intensity (I), the power bandwidth is twice the magnitude order of the light intensity as a logarithmic scale. In the present study, optical bandwidth is considered. According to the Fig. 11, the calculated bandwidth is equal to 35 MHz; the red curve indicates the points allowed for use in the frequency range:

4 Conclusion

The phenomenon of slow light in physics leads to create a delay in an optical telecommunication cable.

This allows us to create a controllable delay and mount the data on the fiber. Also, by combining controlled delay and an optical router, data can be transferred to other places.

Table 1 Storage time calculation based on physical parameters

NO	δ_1 Detuning (μev)	ω_{21} Detuning (μev)	Tunnelling coupling (μev)	Storage Time (ps)
1	0.5	- 0.5	5	45.3229
2	1	- 1	5	45.4132
3	0.5	- 0.5	3	124.7567
4	1	- 1	3	125.4395
5	0.5	- 0.5	1	792.9443
6	1	- 1	1	809.3398

In this paper, by searching for the deceleration coefficient in terms of the identified physical parameters δ_1 and T_e , we have reached a point with an SDF of 3.2×10^6 , where the group speed is less than 100 m per second (93.75 m/s). This means that the speed of light in these physical parameters is also slower than that of sound in the medium. In the present work, the SDF has increased significantly compared to the previous research.

Funding The authors have not disclosed any funding.

Declarations

Conflict of interest The authors declare that they have no known competing financial interests or personal relationships that could have appeared to influence the work reported in this paper.

References

- Abdolhosseini, S., Kohandani, R., Kaatuzian, H.: Analysis and investigation of temperature and hydrostatic pressure effects on optical characteristics of multiple quantum well slow-light devices. *Appl. Opt.* **56**(26) (2017). <https://doi.org/10.1364/AO.56.007331>
- Borges, H.S., Sanz, L., Villas-Bôas, J.M., Diniz Neto, O.O., Alcalde, A.M.: Tunneling induced transparency and slow light in quantum dot molecules. *Phys. Rev. B* **85**, 115425 (2012)
- Chang-Hasnain, C.J., Ku, P.C., Kim, J., Chuang, S.L.: Variable optical buffer using slow light in semiconductor nanostructures. *Proc. IEEE* **91**, 1884 (2003)
- Ficek, Z., Swain, S.: Quantum interference in optical fields and atomic radiation. *J. Mod. Opt.* **49**, 3 (2002). <https://doi.org/10.1080/09500340110065781>
- Fleischhauer, M., Imamoglu, A., Marangos, J.P.: Electromagnetically induced transparency: Optics in coherent media. *Rev. Mod. Phys.* **77**, 633 (2005). <https://doi.org/10.1103/RevModPhys.77.633>
- Fritze, M., Cheetham, P., Lato, J., Syers, P.: The Death of Moore's Law. (n.d.)
- Harris, S.E.: Electromagnetically induced transparency. *Phys. Today* **50**, 36 (1997). <https://doi.org/10.1063/1.881806>
- Hayashida, N., Hirata, H., Komaki, T., Usami, M., Ushida, T., Itoh, H., Yoneyama, K., Utsunomiya, H.: *Jpn. J. Appl. Phys.* **42**, 750–753 (2003)
- Kaatuzian, H.: Nano-refraction Analysis for Advanced Materials: A Theoretical Roadmap for Quantum Computers. *Adv. Mater. Sci. Technol.* **2**, 2. K. (2020a). <https://doi.org/10.37155/2717-526X-0202-1>
- Kaatuzian, H.: Photonic volume2. AKU press, fifth printing. (2020b)
- Li, X., Wang, T., Dong, C.: Reduction of Pure Dephasing Rates of Excitons by Population Decay in Quantum-Dot Semiconductor Optical Amplifiers. *IEEE J. Quantum. Electron.* **50**(7) (2014). <https://doi.org/10.1109/JQE.2014.2326182>
- Marangos, J.P.: Electromagnetically induced transparency. *J. Mod. Opt.* **45**, 471 (1998). <https://doi.org/10.1080/09500349808231909>
- Xiao, Y., Klein, M., Hohensee, M., Jiang, L., Phillips, D.F., Lukin, M.D., Walsworth, R.L.: Slow Light Beam Splitter. *Phys. Rev. Lett.* **101**, 043601 (2008)

Publisher's note Springer Nature remains neutral with regard to jurisdictional claims in published maps and institutional affiliations.